Indentation-induced stress distribution and pressure effect on the resistivity of YSZ

Yusuke Daiko[*,a], *Eri Takahashi*[b], *Yann Gueguen*[c], *Hiroyuki Muto*[d], *Atsunori Matsuda*[d], *Tetsuo Yazawa*[b], *Tanguy Rouxel*[c], *Yuji Iwamoto*[a]

[a] Department of Frontier Materials, Nagoya Institute of Technology, Gokiso-cho, Showa-ku, Nagoya, Aichi 466-8555, Japan

[b] Department of Materials Science and Chemistry, University of Hyogo, 2167 Shosha, Himeji, Hyogo 671-2280, Japan

[c] Mechanics and Glasses Department, IPR, UMR -CNRS 6251, Université de Rennes 1, Campus de Beaulieu, Rennes Cedex, 35042, France

[d] Department of Electrical and Electronic Information Engineering, Toyohashi University of Technology, 1-1 Hibarigaoka, Tempaku-cho, Toyohashi, Aichi 441-8580, Japan

***Corresponding Author**

E-mail: daiko.yusuke@nitech.ac.jp

ABSTRACT

Ionic conductivities measured under GPa-order high pressure provide various information about ion hopping mechanisms such as the activation volume (ΔV). Traditionally, anvil cells have been used for high-pressure measurements. We previously reported a new method for high-pressure impedance measurements, up to a few GPa, employing an indentation-induced local stress field. In this method, both mechanical and electrical (Young's modulus and high pressure impedance) properties can be obtained simultaneously. However, in this method, high pressures are induced only around the tip of the indenter, and such stress distribution should be considered for the estimation of ΔV accurately. In the present study, employing a finite element method (FEM) calculation, the stress distribution around the tip of the indenter, and effects of such GPa-order high pressures on the O^{2-} ion conduction are shown.

Keywords:

Indentation, Activation volume, Fuel cell, Y_2O_3-doped zirconia, Hertz theory

1. INTRODUCTION

Electrochemical analysis of conducting and dielectric materials under high pressures has received considerable attention in view of various interesting properties such as crystallographic phase transition, shifts of temperatures (Curie point/superconducting transition) and changes in phonon modes [1-9]. For ionic conductors, conductivity, σ, is expressed as

$$\sigma = \sigma_0 \, exp \, \{-(\Delta E + p\Delta V) / RT \}, \qquad (1)$$

where σ_0 is a pre-exponential factor [S/cm], ΔE is the activation energy [J/mol], p is the pressure [Pa], ΔV is the activation volume [cm^3/mol], R is the gas constant [J/mol·k], and T is the absolute temperature [k]. The respective derivative forms of ΔE and ΔV are

$$\Delta E = -RT\{d(ln\sigma) / d(T^{-1})\}_p, \qquad (2)$$

$$\Delta V = -RT\{d(ln\sigma) / dp\}_T. \qquad (3)$$

According to the temperature dependence of conductivity, at a constant pressure (e.g., 0.1 MPa of ambient pressure), ΔE can be obtained from Eq. **(2)**. The ΔE is correlated with the energy barrier for ion hopping from a site to an adjacent site. Similarly, from the pressure dependence of conductivity at a constant temperature, ΔV can be obtained. ΔV is identified with local relaxation that accompanies the opening up of sites to admit incoming ions [10-16]. A solid electrolyte of α-AgI that readily conducts Ag^+ ions has a relatively small value of ΔV (~0.9 cm^3/mol) [12], whereas the typical ionic crystal KCl poorly conducts K^+ ions and has a reported ΔV of ~8.0 cm^3/mol [10].

Essentially, ΔE has only positive values, while ΔV has both positive and negative values. For example, ΔV for the rate constant k of ammonia synthesis (Haber-Bosch process) is a negative value, suggesting the rate for ammonia synthesis increases with increasing pressure. Additionally, ΔV for electron including small polaron conductions are usually a

negative value [17], and electron conductivity increases with increasing pressure owing to the overlap of wave functions. It has been reported that some ionic conductors such as Li^+ ion-substituted β-Al_2O_3 have negative ΔV values, which correspond to an increase in conductivity with increasing pressure [18]. Evaluations of both ΔE and ΔV are thus important to understand the ion conduction mechanism in detail and also to screen a new type of electrolyte. However, high pressures of GPa order are usually indispensable for ΔV analysis of solid electrolyte, and high-pressure apparatuses such as diamond anvil cells are necessary for measurement [19,20]. Although the importance of ΔV measurements has been suggested in some literatures [10-16], few papers have reported experimental data for ΔV, likely because of the difficulties and limitations associated with conventional high-pressure methods including the calibration of pressure, sample preparation (involving small sample sizes of ~0.001 cm^3) and temperature increase up to a few hundred °C. In addition, measurements are often performed under a fixed atmosphere, which does not allow evaluation of impedance under various atmospheres (e.g., it is difficult to switch the measurement condition from an oxygen to hydrogen (fuel cell) atmosphere in the case for utilizing a diamond anvil cell).

We previously reported a new GPa-order high-pressure impedance measurement based on an indentation technique [21]. Indentation techniques have been widely used for the analysis of mechanical properties such as the elastic modulus, hardness and viscosity [22-26]. An important point about this method is that the indentation-induced local stress reaches values scaling with hardness, i.e. of a few GPa, and we have tried to utilize this local stress field induced around the tip of the indenter for high-pressure impedance measurement. The value of ΔV for 10 mol% Y_2O_3-doped zirconia (YSZ) was estimated to be around 3.9 cm^3/mol [21]. ΔV increases with increasing temperature, and a similar behavior was reported

for typical electrolytes [11,12,27], as well as for creep viscosity measurements in glasses and polymers [28,29].

Employing the above method, ΔV can be easily and rapidly obtained without any pressure mediums or pressure calibrations. In this indentation method, however, GPa-order high pressure is induced only around the tip of the indenter. Thus, the stress distribution should be considered in order to estimate the effect of high pressure for O^{2-} ion conduction accurately. As such, no physical correlation can be drawn between ΔV values obtained under uniform stress (e.g., using an anvil cell) and those obtained under local stress (indentation) conditions.

In this study, the stress distribution around the tip of an indenter and its effect on the conduction for O^{2-} ion hopping were estimated using a finite element method (FEM) considering both linear elasticity for the mechanical behavior and Eq. (1) for the conductivity, and the simulation results were compared with experimental data. ΔV of YSZ is discussed in relation to the stress distribution.

2. Experimental

Yttria-doped zirconia (10 mol% Y_2O_3, TOSOH Co., Japan) (10YSZ) was used as the test material. 10YSZ powder (0.8 g) was pelletized (13 mm in diameter) at 25 kN and room temperature, and subsequently sintered at 1500 °C for 1 h. The obtained sample was mirror-polished using a diamond slurry (0.25-μm diamond, IMT Co., Ltd., Japan). The indentation measurements were performed using a hand-made indentation apparatus [21]. A spherical Inconel625 indenter was used in the case for the measurement of high-pressure impedance. As shown in Fig. 1, the Inconel indenter plays the role of a collecting electrode simultaneously. The curvature radius of the Inconel indenter was 0.5 mm. A gold ring electrode was sputtered on the 10YSZ. The electrical resistance for O^{2-} ion conduction

between the ring electrode and indenter was measured using an LCR meter (ZM2376, NF Corporation, Japan) at frequencies ranging from 10 kHz to 20 Hz and 1 V under a nitrogen gas atmosphere that prevented oxidation of the apparatus.

Finite element simulation software (COMSOL Multiphysics® ver. 5.1 with AC/DC and structural mechanics modules) was used for the simulation of the stress distribution and of the resistance according to Eq. (1). Parameters for the simulation are summarized in Table 1. The activation energy for 10YSZ was reported to be ≈100 kJ/mol and 80 kJ/mol at temperatures around 500°C and above 800°C, and 100 kJ/mol was substituted into the ΔE of Eq. (1) for the FEM calculation [30-33]. An axially symmetric two-dimensional model was used; the sample geometry is shown in Fig. 2. All sizes of the sample, ring electrode, and indenter were exactly the same as for the experimental condition of indentation. The indenter and YSZ constituted a contact pair, and boundary conditions of contact and continuity were used for structural mechanics and AC/DC modules, respectively. A point load from 1 to 25 N was applied at P_2 in Fig. 2**.** The mesh used for the finite element analysis is shown in Fig. 3. Triangle and square elements were used in order to reduce the calculation time effectively; the numbers of element were 10035 and 1736, respectively.

3. Results and discussion

3.1 Hertz's elastic theory for YSZ

Indentation techniques, measuring the relationship between the load (P) and penetration depth (h), have been widely used for the analysis of mechanical properties, and *e.g.* the elastic modulus, yield strength, hardness as well as time-dependent-viscoelastic parameters can be obtained [22-26,34]. We have used a spherical indenter in order to vary the contact pressure easily. Note that the contact pressure changes by changing the indentation load only in the elastic deformation regime when a spherical indenter is used, since the

contact pressure becomes load independent when a permanent deformation occurs. The indentation load was stepwise increased from 0 to 25 N, and the load was kept at constant values (5, 10, 15, 20 and 25 N) for 100 s, and impedance measurement was performed during the constant loads using an LCR meter.

The relationship between the load (P) [N] and penetration depth (h) [μm] at 500°C is shown in Fig. 4a. The dot-line represents the result of fitting based on the Hertz's elastic model. It is clear that the line is well-fitted on the experimental P-h curve:

$$P = 4/3\ E^{*}\ r^{1/2}\ h^{3/2} \tag{4}$$

$$E^{*} = \{(1 - \nu_s^2) / E_s + (1 - \nu_i^2) / E_i\}^{-1} \tag{5}$$

where r is the curvature radius of the spherical indenter (r = 0.5 mm), E^{*} is the effective elastic modulus, E and ν are the Young's modulus and Poisson's ratio, and the subscripts s and i refer to the sample and indenter, respectively. Also, the loading and unloading curves are exactly overlapped using the spherical indenter at 500°C, suggesting a full elastic deformation of the 10YSZ under the measurement condition. Thus, the indentation behavior was analyzed based on the Hertz's elastic model. No cracks or other damage were seen in either the 10YSZ or the indenter after the test.

According to the data, the Young's modulus and Poisson's ratio of Inconel625 are ≈180 GPa and 0.3 at 500°C [35,36]. The Poisson's ratio of 10YSZ was reported to be ≈0.3 [37]. By assuming the value of the Poisson's ratio ν = 0.3 for 10YSZ, the Young's modulus of 10YSZ was estimated to be 150 GPa at 500°C from the equations (4) and (5). Similar values have also been reported [38]. One big advantage compared with the traditional high-pressure test (e.g. diamond anvil cell) is that the mechanical and electrical properties can be simultaneously estimated in our indentation method.

Here it should be mentioned that the yield strength of Inconel625 is depending on some treatments including the aging temperature and time, and the value was reported to be

less than 1 GPa at 500°C [35,36]. In some cases, the E^* obtained from *P-h* curve (Fig. 4a) changed slightly after using the same Inconel indenter several times. A mechanical damage for the Inconel indenter may occur. The indenter was thus changed frequently. Recently, a harder material with a good conductivity such as boron-doped diamond has also been used for indentation/conductivity analysis [39].

3.2 Stress distribution and resistance

In our indentation method, the GPa order high pressure is induced only around the tip of indenter. The conductivity was previously calculated using the resistance, the contact area of the indenter, and the distance between the indenter and ring-electrode [21]. The activation volumes of ≈3.9 cm^3/mol were obtained from the slope of conductivity ($\log \sigma$) vs pressure. In this calculation, however, we ignored the stress distribution for the calculation of conductivity, and such stress distribution should be considered for the estimation of ΔV accurately. In the present study, we used a finite element method (FEM) to clarify the effect of the local-induced high pressure for ion conduction. Fig. 4b shows the *P-h* curve obtained using the FEM calculation. The same *P-h* curve for Hertz's elastic model in Fig. 4a is also replotted. It is clear that these three *P-h* curves are in good agreement to each other.

Fig. 5a shows the 2D view of the pressure at Gauss point calculated by the FEM (P = 25 N), and the relationship between the distance (x) from the tip of indenter and the pressure on the YSZ surface (y = 0 in Fig. 5a) is shown in Fig. 5b (1D view). Note that approximately 5 GPa is induced at the contact region between Inconel and YSZ. The pressure decreases drastically with increasing the distance x, and the high pressure region disappears over x = 0.05 mm.

We calculated the maximum pressure (Hertz's pressure, p [Pa]) from the penetration depth h as follows:

$$a_c = (r \cdot h)^{1/2} \quad (6)$$

$$p = 3P / 2\pi a_c^2 \quad (7)$$

where a_c is the contact radius of the indenter [m^2]. Relationships between the indentation load and contact pressure, calculated using the experimentally measured penetration depth (Eq. (6) and (7)) or FEM calculation, are shown in Fig. 6. It is evident that the FEM calculation is in very good agreement with experimental results, suggesting a suitable mesh and parameters of FEM calculation.

The obtained pressure at the Gauss point of each node was substituted into the p of Eq. (1), and conductivity of 10YSZ was defined as a function of the pressure, followed by the FEM calculation of the current density [A/m^2]. For the FEM calculation, 1 V was applied between the indenter and ring electrodes. The current [A] was obtained by the integration of the current density with the area of ring-electrode. Here, σ_0 and ΔV were varied, and we compared the resistivities between experimental (LCR) and FEM calculation for various σ_0 and ΔV.

Typical Cole-Cole plot is shown in Fig. 7. The resistance at a resonant frequency shown as the arrow (the first semicircle) was adopted. Since our sample was not single crystal, the resistance is considered to be included both grain and grain boundary resistances. In this study, we focused only bulk (grain and grain boundary) resistance. Note the bulk resistance decreases, while the estimated contact area increases with increasing the load from 5 to 25 N. As shown in Fig. 1, the Inconel indenter also plays the role of a collecting electrode. Since the hopping of O^{2-} ions occurs between the indenter and ring electrodes, such a small high-pressure region should affects on the resistance for O^{2-} conduction.

Typical results of the resistance of the experimental data and FEM calculation are shown in **Fig. 8**. The ΔV value affects significantly on resistance at higher load. The

differences (δ) of resistances between experimental and FEM calculation were estimated as follow:

$$\delta = \sum (R_{\text{experimental}} - R_{\text{FEM}})^2 \qquad (8)$$

where $R_{\text{experimental}}$ and R_{FEM} are resistances obtained from experiment and FEM calculation, respectively. In the case of ΔV = 0 cm^3/mol, the FEM calculation is in agreement with experimental data in lower loads, whereas a deviation is clearly seen over 15 N (corresponding to that over ~4 GPa from **Fig. 6)**. A smaller δ value was obtained for ΔV = 3.5 cm^3/mol as compared with the case for ΔV = 2.0 cm^3/mol, suggesting that the ΔV of 10YSZ is around 3.5 cm^3/mol at 500°C.

In any cases for ΔV from 0 to 3.5 cm^3/mol, the σ_0 was estimated to be around 2000 ~ 2300 S/cm. The σ_0 is composed of several terms including the average jump distance squared, the density of charge carriers and the attempt frequency of the jumping atom *etc*. The Meyer-Neldel (MN) rule has been widely studied since its discovery in 1937. The MN rule can be applied for various activated hopping systems including electron/hole conduction of semiconductors, ionic conduction as well as thermally activated hopping and so on [40]. According to the NM rule, a linear relationship can be seen between the activation energy and log σ_0, and various materials obey the NM rule [40]. The relationship between the logσ_0 and ΔE for YSZ measured at various temperatures and compositions (varied the amount of Y_2O_3) is plotted in Fig. 9. Note that the FEM calculation result (σ_0 = 2300 S/cm at ΔE = 100 kJ/mol) is in very good agreement with the NM correlation for YSZ, and thus we conclude the σ_0 calculated is also reasonable.

A estimation of the activation volume, ΔV, can be obtained easily and rapidly by just fitting the experimentally obtained resistance data based on the Eq. **(1),** once the stress distribution around the tip of the indenter is accounted for using FEM for instance. It should be mentioned, however, the experimental error for the resistance becomes notable in lower

load (see Fig. 8), maybe due to very small value of the contact area. As shown in Fig. 6, the pressure increases drastically from 0 up to 5 N. In Fig. 10, the FEM calculation results for the ΔV = 2.0 and 3.5 cm^3/mol in Fig. 8 are replotted for comparison. Note the effect on the local stress around the tip of indenter become more significant below 10 N. Our experimental and calculation results suggest that a precise indentation measurement for resistance in the region 0 to 10 N of load is necessary in order to evaluate the ΔV precisely. Further improvement for the indentation measurement, especially about the indentation test under lower load-region is in progress. Also, the comparison of ΔV obtained under uniform stress (e.g., using an anvil cell) and those obtained under local stress (indentation) conditions is under studying.

4. Conclusion

The pressure effect on the O^{2-} conduction of YSZ was measured by using an indentation apparatus, and experimentally obtained resistance is discussed in relation with the FEM calculation. The *P-h* profile curve was obtained with a good reproducibility and accuracy, and profile data was well fitted by the Hertz's theoretical values. The indentation induced high-pressure stress field can be applied for the estimation of ΔV, and the ΔV of 3.5 cm^3/mol was obtained by considering the stress distribution around the tip of indenter using the finite element method. Compared with conventional techniques for the calculation of ΔV, the apparatus we developed is very simple, performs rapid analysis, and mechanical and electrical properties are obtained simultaneously.

Acknowledgment

This work was financially supported by the Ministry of Education, Culture, Sports, Science and Technology (Japan) (No. 23686095, No. 15H04124) and by Toyota Physical and Chemical Research Institute Scholars.

REFERENCES

[1] R.K. Chan, D.W. Davidson, E. Whalley, J. Chem. Phys. 43 (1965) 2376.

[2] G.A. Samara, Phys. Rev. B 27 (1983) 3494.

[3] I.N. Goncharenko, I. Mirebeau, Phys. Rev. Lett. 80 (1998) 1082.

[4] H. Karzel, W. Potzel, M. Köfferlein, W. Schiessl, M. Steiner, U. Hiller, G.M. Kalvius, D.W. Mitchell, T.P. Das, P. Blaha, K. Schwarz, M.P. Pasternak, Phys. Rev. B 53 (1996) 11425.

[5] S. Sadewasser, J.S. Schilling, A.P. Paulikas, B.W. Veal, Phys. Rev. B 61 (2000) 741.

[6] F. Iguchi, S. Onodera, N. Sata, H. Yugami, Solid State Ionics 225 (2012) 99.

[7] D.A. Boysen, S.M. Haile, H. Liu, R.A. Secco, Chem. Mater. 15 (2003) 727.

[8] H. Takahashi, K. Igawa, K. Arii, Y. Kamihara, M. Hirano, H. Hosono, Nature 453 (2008) 376.

[9] G.A. Samara, Phys. Rev. 151 (1966) 378.

[10] D.N. Yoon, D. Lazarus, Phys. Rev. B 5 (1972) 4935.

[11] P.C. Allen, D. Lazarus, Phys. Rev. B 17 (1978) 1913.

[12] B.-E. Mellander, Phys. Rev. B 26 (1982) 5886.

[13] A. Bunde, M.D. Ingram, S. Russ, Phys. Chem. Chem. Phys. 6 (2004) 3663.

[14] G.A. Samara, Solid State Phys. 38 (1984) 1.

[15] R. Hinrichs, G. Tomandl, J.A.H. da Jornada, Solid State Ionics 77 (1995) 257.

[16] Q. Chen, A. Braun, S. Yoon, N. Bagdassarov, T. Graule, J. Eur. Ceram. Soc. 31 (2011) 2657.

[17] A. Goddat, J. Peyronneau, J.P. Poirier, Phys. Chem. Miner. 27 (1999) 81.

[18] R.H. Radzilowski, T. Kummer, J. Electrochem. Soc. 118 (1971) 714.

[19] A. Hao, C. Gao, M. Li, C. He, X. Huang, G. Zou, Y. Tian, Y. Ma, J. Appl. Phys. 101 (2007) 053701.

[20] S. Matsuzaki, Synthetic Metals 61 (1993) 207.

[21] Y. Daiko, E. Takahashi, N. Hakiri, H. Muto, A. Matsuda, T. Rouxel, J.-C. Sangleboeuf, A. Mineshige, T. Yazawa, Solid State Ionics 254 (2014) 6.

[22] G.M. Pharr, Mater. Sci. Eng. A 253 (1998) 151.

[23] S. Yoshida, J.-C. Sangleboeuf, T. Rouxel, J. Mater. Res. 20(12) (2005) 3404.

[24] B.R. Lawn, A.G. Evans, D.B. Marshall, J. Am. Ceram. Soc. 63 (1980) 574.

[25] J.-J. Kim, Y. Choi, S. Suresh, A.S. Argon, Science 295 (2002) 654.

[26] R. Saha, W.D. Nix, Acta Mater. 50 (2002) 23.

[27] M.D. Ingram, C. T. Imrie, I. Konidakis, S. Voss, Phys. Chem. Chem. Phys. 6 (2004) 3659.

[28] T. Rouxel, M. Huger and J.L. Besson, J. Mat. Sci. 27 (1992) 279.

[29] J.C. Cavrot, J. Haussy, J.M. Lefebvre, B. Escaig, Mater. Sci. Eng. 36 (1978) 95.

[30] A. Pimenov, U. Ulrich, P. Lunkenheimer, A. Loidl, C.H. Rüscher, Soli State Ionic 109 (1998) 111.

[31] G. Chiodelli, A. Magistris, J. Mater. Sci. 23 (1998) 1159.

[32] M.J. Verkerk, B.J. Middelhuis, A.J. Burggraaf, Solid State Ionics 6 (1982) 159.

[33] S.P.S. Badwal, Solid State Ionics 52 (1992) 23.

[34] M. Sakai, S. Shimizu, J. Non-Cryst. Solids 282 (2002) 236.

[35] http://www.specialmetals.com/ (SPECIAL METALS, Inconel alloy 625 ResearchGate)

[36] http://www.jacquet.biz/JACQUET/USA/files/JCQusa-alloy-625.pdf (Alloy625datasheet)

[37] S. Sakaguchi, N. Murayama, Y. Kodama, F. Wakai, J. Mater. Sci. Lett. 10 (1991) 282.

[38] S. Giraud, J. Canel, J. Eur. Ceram. Soc. 28 (2008) 77.

[39] S. Ruffell, J.E. Bradby, J.S. Williams, O.L Warren, J. Mater. Res. 22 (2007) 578.

[40] A. Dalvi, N.P. Reddy, S.C. Agarwal, Solid State Comm. 152 (2012) 612.

[41] A. Pimenov, J. Ullrich, P. Lunkenheimer, A. Loidl, C.H. Rüscher, Solid State Ionics 109 (1998) 111.

[42] G. Chiodelli, A. Magistris, J. Mater. Sci. 23 (1988) 1159.

[43] M.J. Verkerk, B.J. Middelhuis, A.J. Burggraaf, Solid State Ionics 6 (1982) 159.

Captions

Table 1. Parameters for FEM calculation.

Figure 1. Photograph of the indenter and ring electrodes for the high-pressure impedance test (TC: thermocouple).

Figure 2. Cross-section and top views of the sample geometry for the FEM calculation.

Figure 3. Mesh used for the finite element method.

Figure 4. (a) *P–h* curve for YSZ at 500°C measured using the spherical Inconel625 indenter, and (b) that obtained by FEM calculation. The red-curves represent the result of calculation based on the Hertz's elastic model.

Figure 5. (a) 2D view of the pressure at Gauss point calculated by the FEM (P = 25 N), and (b) the relationship between the distance (x) from the tip of indenter and the pressure on the 10YSZ surface (y = 0 in Fig. 5a).

Figure 6. Relationships between the indentation load and contact pressure at 500°C, calculated using the experimentally measured penetration depth (Eq. (6) and (7)) and FEM.

Figure 7. Cole–Cole plots of 10YSZ at 500 °C and 5 N for the ring electrode. The resistance shown by the arrow (the first semicircle) was used for the calculation of conductivity.

Figure 8. Comparison of the resistance between experimental data and FEM calculation at different ΔV from 5 to 25 N. The symbol (●) and line show the results of experimental and FEM calculations, respectively.

Figure 9. Relationship between the ΔE and $\log\sigma_0$ for YSZ measured at various temperatures and compositions (varied the amount of Y_2O_3); ●: the FEM calculation result, Δ: ref[43], ▲: ref [42] (High temperature), ○: ref[41], ▼: ref[42] (Low temperature).

Figure 10. FEM calculation results for ΔV = 2.0 and 3.5 (re-plot the curves shown in Fig. 8)

Table 1

Parameters for FEM calculation.

Parameter	Value
Curvature radius of the Inconel indenter	0.5 mm
Young's modulus of YSZ	190 GPa
Young's modulus of Inconel	179 GPa
Poisson's ratio (Inconel, YSZ)	0.3
Density of YSZ	5.8 g/cm^3
Density of Inconel	9.0 g/cm^3
Load	1 ~ 25 N
Conductivity of Inconel	10^5 S/m
ΔE	100 kJ/mol

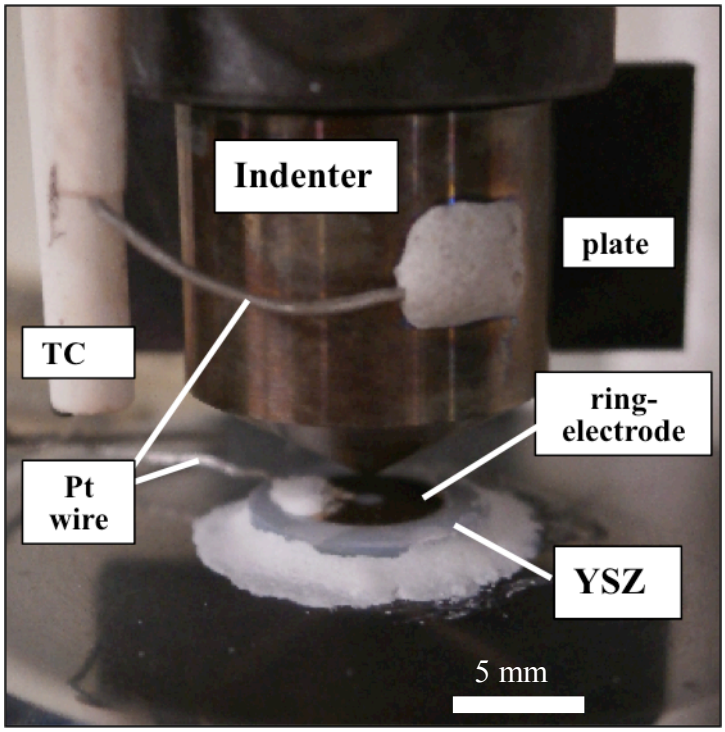

Figure 1

Photograph of the indenter and ring-electrodes for the high-pressure impedance test (TC: thermocouple, bar 5 mm).

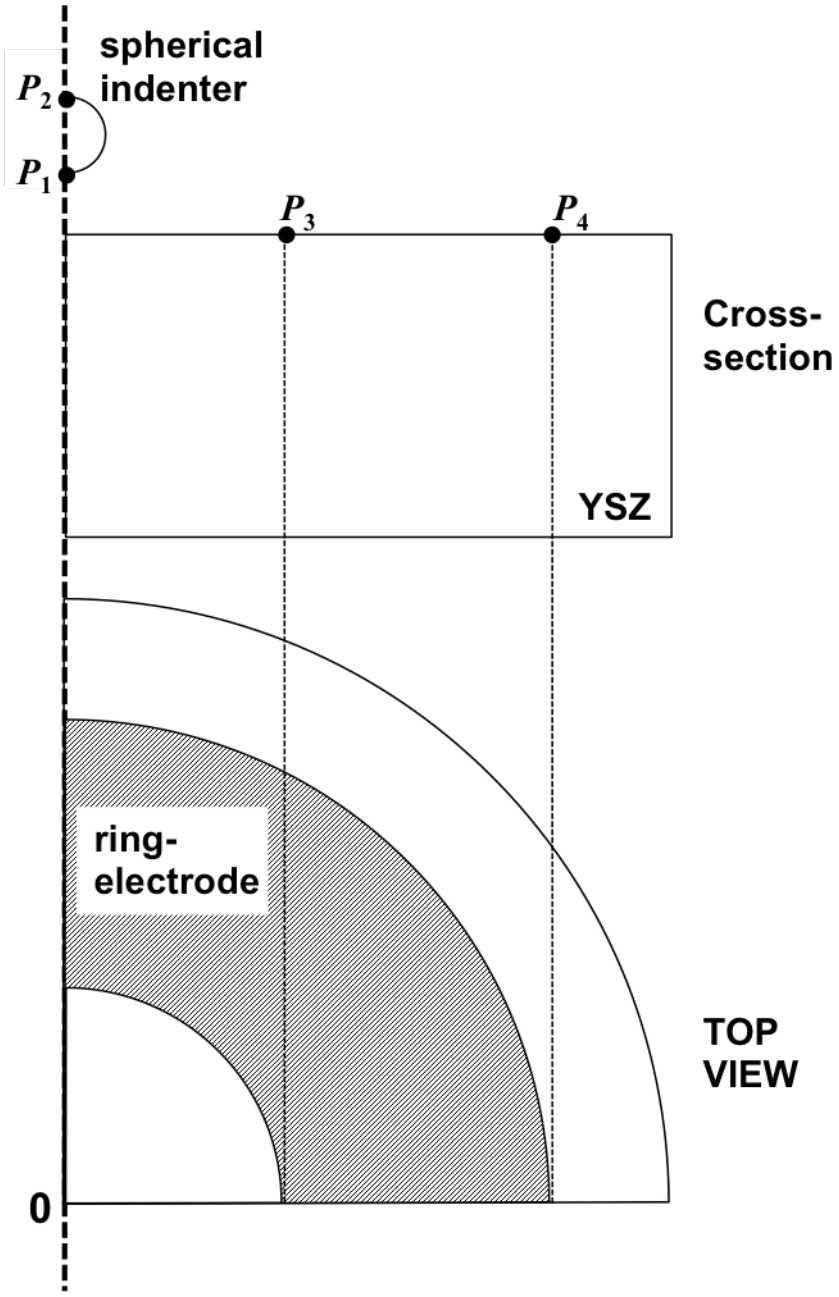

Figure 2

Cross-section and top views of the sample geometry for the FEM calculation.

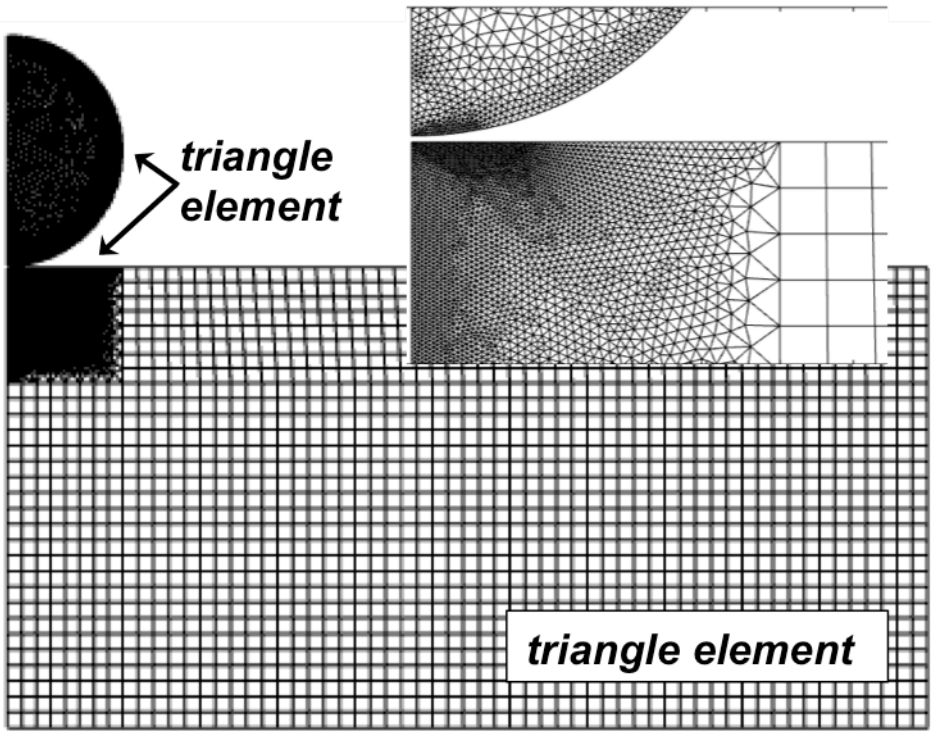

Figure 3

The mesh used for the finite element method.

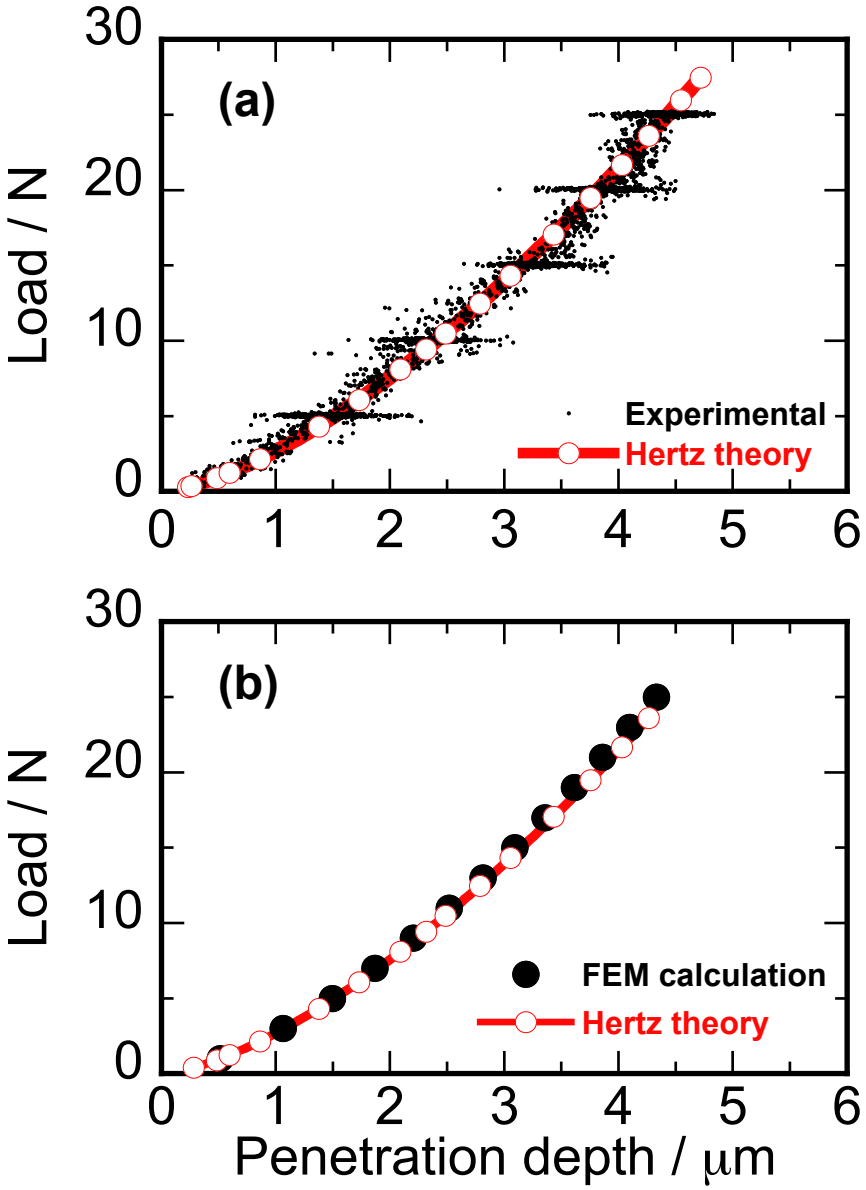
(a)
Load / N
Experimental
Hertz theory
(b)
FEM calculation
Hertz theory
Penetration depth / μm

Figure 4

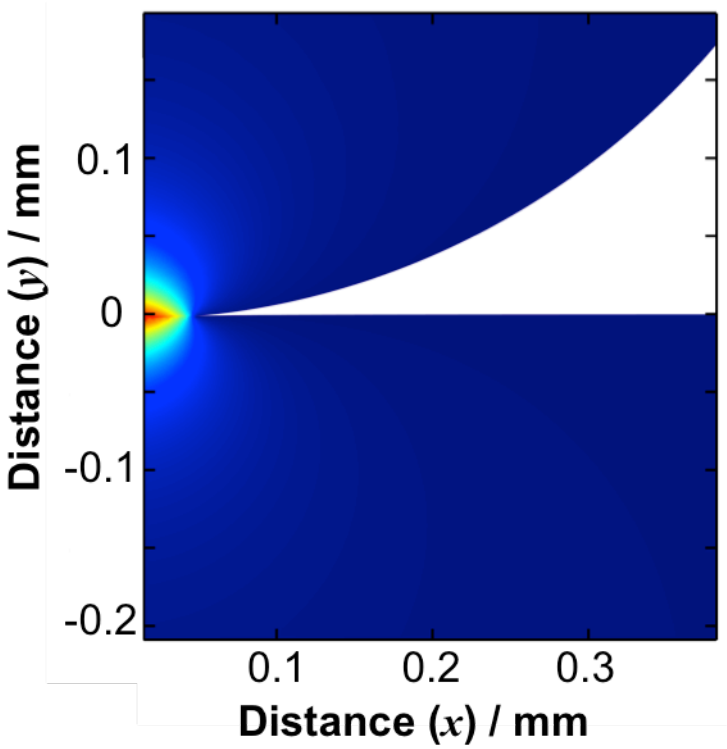

Figure 5a

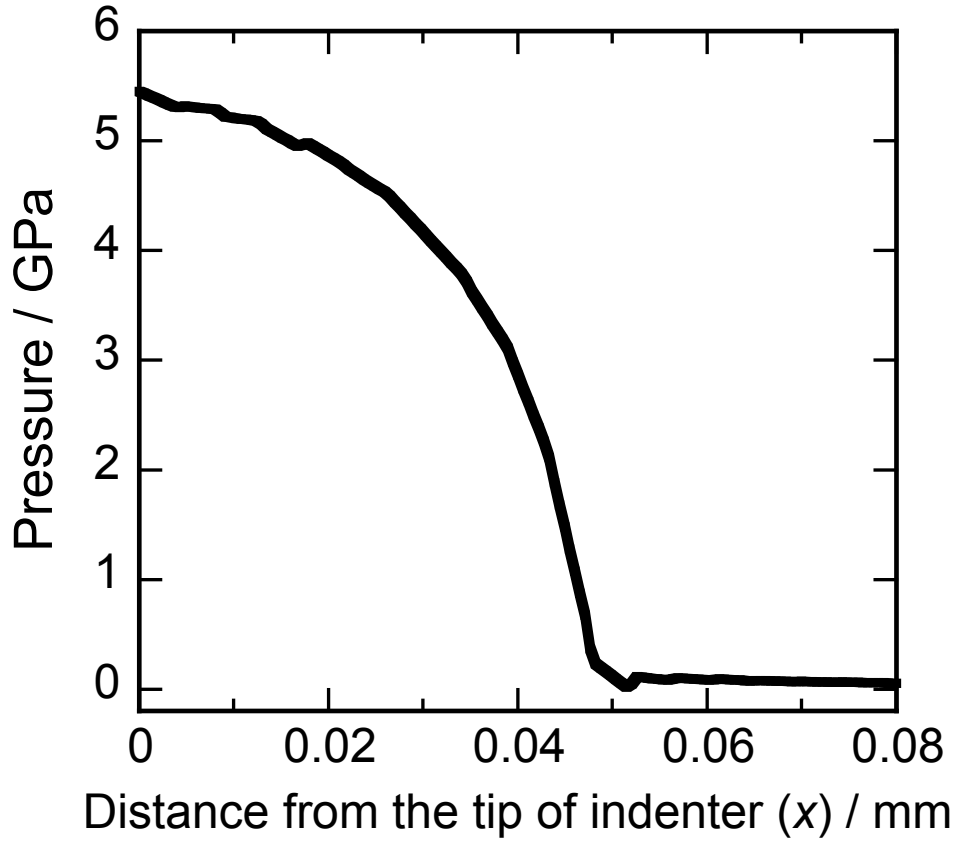
Pressure / GPa
0
1
2
3
4
5
6
0
0.02
0.04
0.06
0.08
Distance from the tip of indenter (x) / mm

Figure 5b

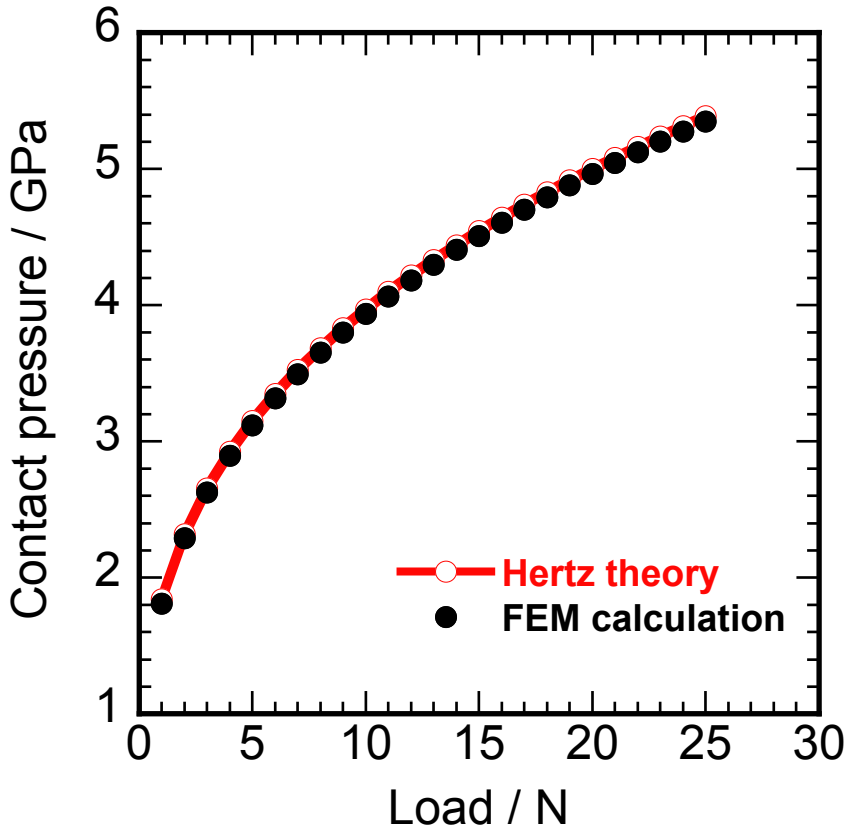
Contact pressure / GPa
Load / N
Hertz theory
FEM calculation
0
5
10
15
20
25
30
1
2
3
4
5
6

Figure 6

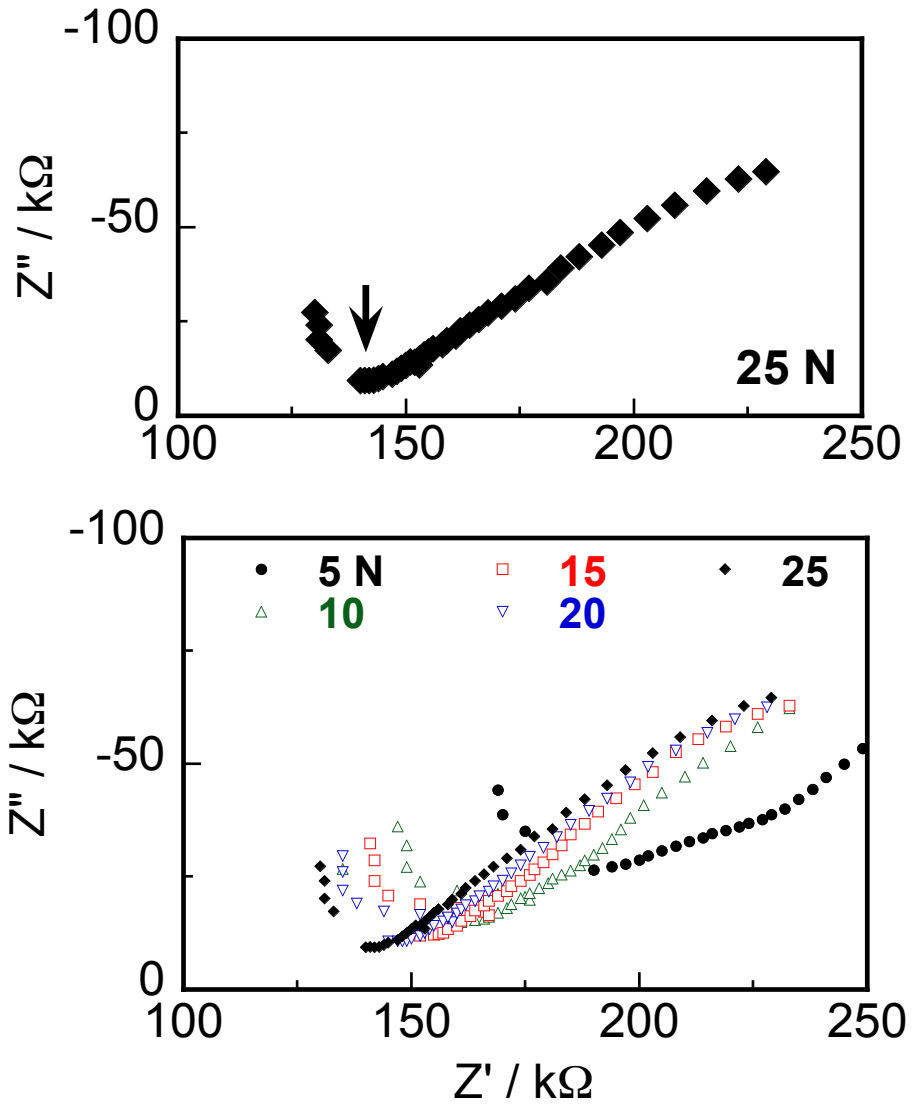

Figure 7

Cole–Cole plots of YSZ at 500 °C and 5 N for the ring electrode. The resistivity shown by the arrow (the first semicircle) was used for the calculation of conductivity.

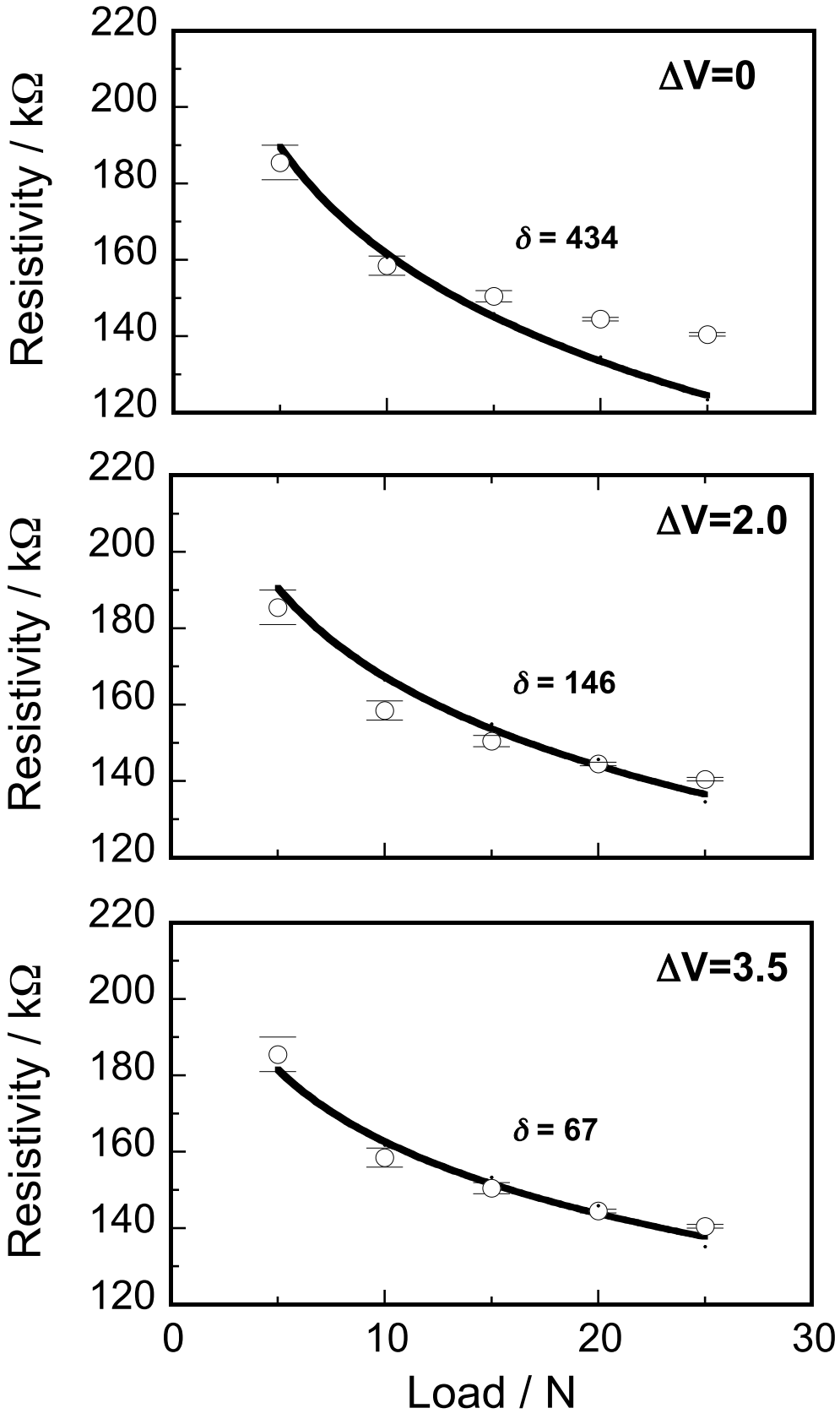
ΔV=0
δ = 434
ΔV=2.0
δ = 146
ΔV=3.5
δ = 67
Resistivity / kΩ
220
200
180
160
140
120
0
10
20
30
Load / N

Fig. 8

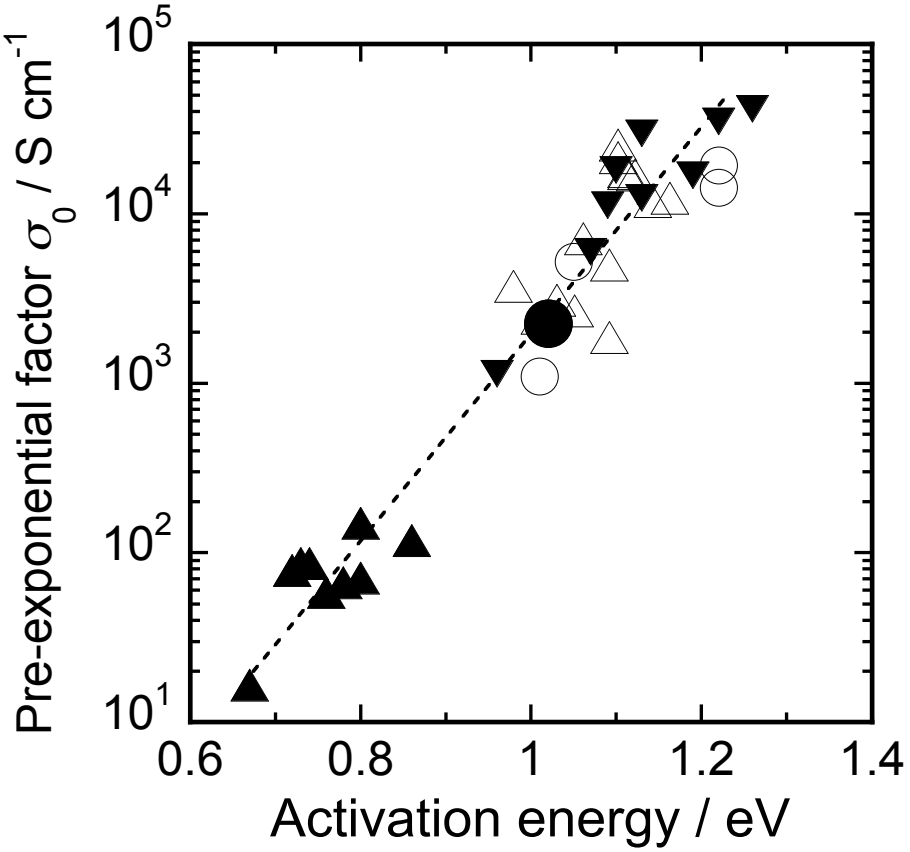
Pre-exponential factor σ_0 / S cm^{-1}
10^5
10^4
10^3
10^2
10^1
0.6
0.8
1
1.2
1.4
Activation energy / eV

Fig. 9

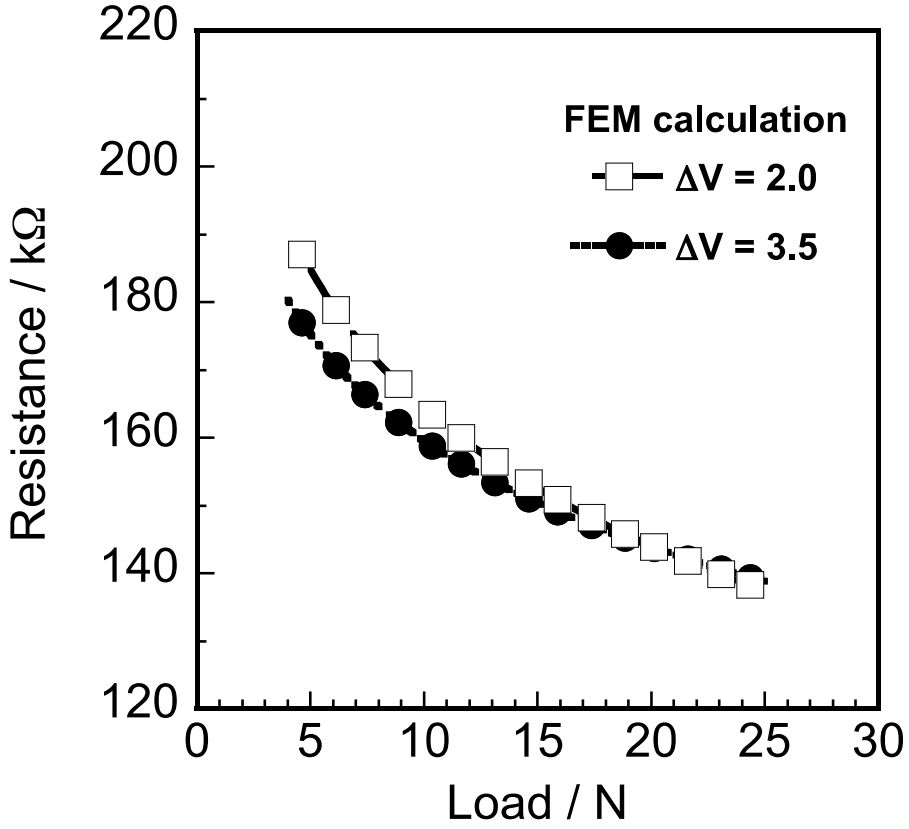
FEM calculation
ΔV = 2.0
ΔV = 3.5
Resistance / kΩ
Load / N
220
200
180
160
140
120
0
5
10
15
20
25
30

Fig. 10